Structural and vibrational study of Bi_2Se_3 under high pressure

Rosario Vilaplana,[1,*] D. Santamaría-Pérez,[2] O. Gomis,[1] F. J. Manjón,[3] J. González,[4,5] A. Segura,[6] A. Muñoz,[7] P. Rodríguez-Hernández,[7] E. Pérez-González,[7] V. Marín-Borrás,[8] V. Muñoz-Sanjose,[8] C. Drasar,[9] and V. Kucek[9]

[1]*Centro de Tecnologías Físicas, MALTA Consolider Team, Universitat Politècnica de València, 46022 Valencia, Spain*

[2]*Departamento de Química Física I, Universidad Complutense de Madrid, MALTA Consolider Team, Avenida Complutense s/n, 28040 Madrid, Spain*

[3]*Instituto de Diseño para la Fabricación y Producción Automatizada, MALTA Consolider Team, Universitat Politècnica de València, 46022 Valencia, Spain*

[4]*DCITIMAC–MALTA Consolider Team, Universidad de Cantabria, Santander, Spain*

[5]*Centro de Estudios de Semiconductores, Universidad de los Andes, Mérida 5201, Venezuela*

[6]*Instituto de Ciencia de Materiales de la Universidad de Valencia–MALTA Consolider Team–Departamento de Física Aplicada, Universitat de València, 46100 Burjassot, Valencia, Spain*

[7]*MALTA Consolider Team–Departamento de Física Fundamental II, Instituto Univ. de Materiales y Nanotecnología, Universidad de La Laguna, La Laguna, Tenerife, Spain*

[8]*Departamento de Física Aplicada, Universitat de València, 46100 Burjassot, Valencia, Spain*

[9]*Faculty of Chemical Technology, Department of Physics, University of Pardubice, Studentská 95, 53210-Pardubice, Czech Republic*

(Received 13 September 2011; published 28 November 2011)

The structural and vibrational properties of bismuth selenide (Bi_2Se_3) have been studied by means of x-ray diffraction and Raman scattering measurements up to 20 and 30 GPa, respectively. The measurements have been complemented with *ab initio* total-energy and lattice dynamics calculations. Our experimental results evidence a phase transition from the low-pressure rhombohedral (R-3m) phase (α-Bi_2Se_3) with sixfold coordination for Bi to a monoclinic $C2/m$ structure (β-Bi_2Se_3) with sevenfold coordination for Bi above 10 GPa. The equation of state and the pressure dependence of the lattice parameters and volume of α and β phases of Bi_2Se_3 are reported. Furthermore, the presence of a pressure-induced electronic topological phase transition in α-Bi_2Se_3 is discussed. Raman measurements evidence that Bi_2Se_3 undergoes two additional phase transitions around 20 and 28 GPa, likely toward a monoclinic $C2/c$ and a disordered body-centered cubic structure with 8-fold and 9- or 10-fold coordination, respectively. These two high-pressure structures are the same as those recently found at high pressures in Bi_2Te_3 and Sb_2Te_3. On pressure release, Bi_2Se_3 reverts to the original rhombohedral phase after considerable hysteresis. Symmetries, frequencies, and pressure coefficients of the Raman and infrared modes in the different phases are reported and discussed.

DOI: 10.1103/PhysRevB.84.184110 PACS number(s): 63.20.−e, 62.50.−p, 78.30.−j

I. INTRODUCTION

Bismuth selenide (Bi_2Se_3) is one of the binary end members of the $(Bi,Sb)_2(Te,Se)_3$ family of semiconductors. These layered chalcogenides have a tremendous impact for thermoelectric applications, which are critical components for solid state power generating and refrigerating devices.[1] Therefore, these semiconductors and their alloys have been extensively studied. However, due to the superiority of Bi_2Te_3-based materials for these applications at room temperature[2,3] and of Sb_2Te_3-based materials in the region between 400K and 500K,[3,4] Bi_2Se_3, while well studied, has not been subjected to the same degree of intensive research that the other two end members of the family have received.

Bi_2Se_3 is a narrow band gap semiconductor with a tetradymite crystal structure (R-3m, space group (SG) 166, $Z = 3$).[5] This rhombohedral layered structure is formed by *quintuple* layers, i.e., formed by five hexagonal close-packed atomic sublayers (Se-Bi-Se-Bi-Se), linked by van der Waals forces. The same structure is common to other narrow band gap semiconductor chalcogenides, like Bi_2Te_3 and Sb_2Te_3, and has been found as a high-pressure phase of As_2Te_3.[6] These materials can be exfoliated like graphene and that a single layer exhibits high electric conductivity and low thermal conductivity, so a new nanostructure route can be envisaged to improve dramatically the thermoelectric properties of this compound by means of either charge carrier confinement or acoustic phonon confinement.[7–12]

Bi_2Se_3, as well as Bi_2Te_3 and Sb_2Te_3, has been predicted to behave as a topological insulator,[13] i.e., part of a new class of materials with unique properties resulting from the relativistic-like character and topological protection of their surface states. These topological insulators are characterized by the presence of a strong spin–orbit (SO) coupling that leads to the opening of a narrow band gap and causes certain topological invariants in the bulk to differ from their values in vacuum. The sudden change of invariants at the interface results in metallic, time reversal invariant surface states whose properties are useful for applications in spintronics and quantum computation.[14,15] Therefore, in the recent years, a number of papers have been devoted to the search for three-dimensional topological insulators among Sb_2Te_3, Bi_2Te_3, and Bi_2Se_3, and different works have observed the features of the topological band structure in the three compounds.[16–18] Furthermore, the bulk and surface conductance in these layered semiconductors can be explored by controlling the Fermi level after proper doping and that could lead to the discovery of new exotic states.[19,20]

High-pressure studies are useful to understand materials properties and design new materials because the increase in

pressure allows reduction of the interatomic distances and fine-tuning of the materials properties. It has been verified that the thermoelectric properties of semiconductor chalcogenides improve with increasing pressure and that the study of the properties of these materials could help in the design of better thermoelectric materials by substituting external pressure by chemical pressure.[21–25] However, there are relatively few studies of layered chalcogenides Sb_2Te_3, Bi_2Te_3, and Bi_2Se_3 under pressure. The electric and thermoelectric properties of Sb_2Te_3, Bi_2Te_3, and Bi_2Se_3, as well as their electronic band structure, have been studied at high pressures,[26–34] and recent high-pressure studies in these compounds have shown a pressure-induced superconductivity[35,36] that has further stimulated high-pressure studies.[37] However, the pressure dependence of many parameters of these layered chalcogenides is still not known.

Structural studies under pressure in the layered chalcogenides Sb_2Te_3, Bi_2Te_3, and Bi_2Se_3 are scarce. The determination of the crystalline structures of these materials at high pressures has been a long-standing puzzle.[22,30,38,39] Only recently have the SGs of the high-pressure phases of Bi_2Te_3 been elucidated by powder x-ray diffraction (XRD) measurements at synchrotron radiation sources,[40,41] especially with the use of particle swarm optimization algorithms for crystal structure prediction.[41] Furthermore, recent high-pressure powder XRD measurements have evidenced a pressure-induced electronic topological transition (ETT) in Bi_2Te_3 around 3.2 GPa as a change in compressibility.[36,38,39,42,43] An ETT or Lifshitz transition occurs when an extreme of the electronic band structure, which is associated to a Van Hove singularity in the density of states, crosses the Fermi energy level.[44] This crossing, which can be driven by pressure, temperature, doping, etc., results in a change in the topology of the Fermi surface that changes the electronic density of states near the Fermi energy. An ETT is a 2.5 transition in the Ehrenfest description of the phase transitions, so no discontinuity of the volume (first derivative of the Gibbs free energy) is seen but a change in the compressibility (second derivative of the Gibbs free energy) is expected in the vicinity of the ETT. Anomalies in the phonon spectrum are also expected for materials undergoing an ETT[45,46] and have been observed in a number of materials,[47–49] as well as in $Sb_{1.5}Bi_{0.5}Te_3$.[38] Raman scattering measurements have confirmed that both Bi_2Te_3 and Sb_2Te_3 exhibit a pressure-induced ETT and that the high-pressure phases of Bi_2Te_3 up to 25 GPa are observed not only in Bi_2Te_3 but also in Sb_2Te_3.[50,51] To our knowledge, there is no experimental high-pressure XRD study on Bi_2Se_3 under pressure reported in the literature, and it remains to be confirmed whether Bi_2Se_3 (1) suffers an ETT like Bi_2Te_3 and Sb_2Te_3 and (2) undergoes the same structural transformations under pressure as Bi_2Te_3 and Sb_2Te_3.

Vibrational studies under pressure in the layered chalcogenides Sb_2Te_3, Bi_2Te_3, and Bi_2Se_3 are scarce and only a few have been recently reported for Sb_2Te_3 and Bi_2Te_3.[50–52] Experimental and theoretical studies of the vibrational properties of Bi_2Se_3 have been reported at room pressure,[53–59] but to our knowledge there is neither an experimental nor a theoretical study of the lattice dynamics properties of Bi_2Se_3 under high pressure. As part of our systematic study of the structural stability and the vibrational properties of the semiconductor chalcogenide family, we report on room temperature powder XRD and Raman scattering measurements in Bi_2Se_3 up to 20 and 30 GPa, respectively, together with total-energy and lattice dynamics *ab initio* calculations at different pressures. We provide evidence of a pressure-induced ETT in the rhombohedral phase of Bi_2Se_3 and confirm that Bi_2Se_3 seems to follow the same sequence of pressure-induced phase transitions as observed in its parent compounds Sb_2Te_3 and Bi_2Te_3.

II. EXPERIMENTAL DETAILS

We used single crystals of *n*-type Bi_2Se_3 that were grown using the Bridgman technique. A polycrystalline ingot was synthesized by the reaction of stoichiometric quantities of the constituting elements (with 5*N* quality). Afterward, the polycrystalline material was annealed and submitted to the growth process in a vertical Bridgman furnace. Preliminary room temperature measurements on single crystalline samples ($15 \times 4 \times 0.3\ mm^3$) yielded in-plane electric resistivity $\rho_{\perp c} = 5.6 \times 10^{-6}$ Ωm and Hall coefficient $R_H(B \| c) = 0.23\ cm^3C^{-1}$. Providing that $n = 1/R_H e$, the latter results gives an electron concentration of $n = 2.7 \cdot 10^{19}\ cm^{-3}$.

Angle-dispersive powder XRD measurements on Bi_2Se_3 were carried out with an Xcalibur diffractometer (Oxford Diffraction). XRD patterns were obtained on a 135-mm Atlas charge-coupled device (CCD) detector placed 110 mm from the sample using $K_{\alpha 1}$:$K_{\alpha 2}$ molybdenum radiation. The x-ray beam was collimated to a diameter of 300 μm. High-pressure measurements on Bi_2Se_3 powder were performed in a modified Merrill-Bassett diamond anvil cell (DAC) up to 20 GPa. The diamond anvils used have a 500-μm culet size. The gray Bi_2Se_3 powder was placed in the 200-μm-diameter hole of the stainless steel gasket preindented to a thickness of 40 μm. Exposure times were typically 1 h. The DAC used for these experiments allows access to an angular range of $4\theta = 50^\circ$. However, only powder patterns below $2\theta = 18.3^\circ$ were considered because of the appearance of the stain steel peaks of the gasket. The background was manually subtracted. The observed intensities were integrated as a function of 2θ to give conventional, one-dimensional diffraction profiles. CrysAlis software, version 171.33.55 (Oxford Diffraction), was used for the data collections and the preliminary reduction of the data. The indexing and refinement of the powder patterns were performed using the PowderCell[60] and FullProf[61] program packages.

For unpolarized room temperature Raman scattering measurements at high pressures, we inserted a small flake of the single crystal ($100 \times 100 \times 5\ \mu m^3$) in a membrane-type DAC. The Raman measurements were performed in backscattering geometry with a power below 2 mW not to burn the sample. In our measurements, we used two setups: (1) a Horiba Jobin Yvon LabRAM high-resolution microspectrometer equipped with a thermoelectric-cooled multichannel CCD detector, a spectral resolution below 2 cm^{-1}, and a HeNe laser (6328-Å line) used for excitation, and (2) a Horiba Jobin Yvon T64000 triple-axis spectrometer with a resolution of 1 cm^{-1} and an Ar-Kr gas laser (6470-Å line) used for excitation.

In both XRD and Raman experiments, we used a 4:1 methanol–ethanol mixture as the pressure-transmitting medium, which ensures hydrostatic conditions up to 10 GPa

TABLE I. Calculated (th.) and experimental (exp.) lattice parameters, zero-pressure bulk modulus (B_0), and its derivative (B_0') of Bi_2Se_3 in the R-3m structure at zero pressure, and calculated lattice parameters of Bi_2Se_3 in the $C2/m$ and $C2/c$ structures at 13.5 and 25.5 GPa, respectively. Experimental and theoretical values reported in the literature are provided for comparison.

	a (Å)	b (Å)	c (Å)	β (°)	B_0 (GPa)	B_0'	Refs.
			α-Bi_2Se_3 (0 GPa)				
exp.	4.123(1)		28.486(1)		53(8)	2.9(2)	[b]
exp.	4.143		28.636				5
th. (GGA-PBEsol)	4.127		28.315		47.8	3.9	[b]
th. (GGA-PBEsol)[a]	4.141		28.124		48.0	4.6	[b]
th. (GGA-PBE)	4.138		28.640				59
th. (GGA-PBE)[a]	4.215		29.828				59
			β-Bi_2Se_3 (13.5 GPa)				
exp.	14.007(6)	3.829(1)	8.471(6)	88.31(4)	66(3)	4.5	[b]
th. (GGA-PBEsol)	13.940	3.792	8.420	89.06	60.4	4.8	[b]
			γ-Bi_2Se_3 (25.5 GPa)				
th. (GGA-PBEsol)	9.128	6.469	7.191	69.42	77.1	2.6	[b]

[a]Calculations including the SO coupling.
[b]This work.

and quasihydrostatic conditions between 10 and 25 GPa.[62,63] Pressure was determined by the ruby luminescence method.[64]

III. *AB INITIO* CALCULATIONS

The structures of the high-pressure phases of Bi_2Te_3 up to 52 GPa have been reported[40,41] and confirmed to occur not only in Bi_2Te_3 but also in Sb_2Te_3 at high pressures.[50,51] The rhombohedral structure (α-Bi_2Te_3) was suggested to transform to the $C2/m$ (β-Bi_2Te_3, SG 12, $Z = 4$) and the $C2/c$ (γ-Bi_2Te_3, SG 15, $Z = 4$) structures above 8.2 and 13.4 GPa, respectively.[41] Furthermore, a fourth phase (δ-Bi_2Te_3) was found above 14.5 GPa and assigned to a disordered body-centered cubic (bcc) structure (Im-3m, SG 229, $Z = 1$).[40,41] To explore the relative stability of these phases in Bi_2Se_3, we performed *ab initio* total-energy calculations within the density functional theory (DFT)[65] using the plane-wave method and the pseudopotential theory with the Vienna *ab initio* simulation package (VASP).[66] We used the projector-augmented wave scheme[67] implemented in this package. A basis set including plane waves up to an energy cutoff of 320 eV was used to achieve highly converged results and an accurate description of the electronic properties. We used the generalized gradient approximation (GGA) for the description of the exchange-correlation energy with the Perdew-Burke-Ernzerhof for solids (PBEsol)[68] prescription. Dense, special k-point sampling for Brillouin zone (BZ) integration was performed to obtain well-converged energies and forces. At each selected volume, the structures were fully relaxed to their equilibrium configuration through the calculation of the forces and the stress tensor. In the relaxed equilibrium configuration, the forces on the atoms are less than 0.002 eV/Å and the deviation of the stress tensor from a diagonal hydrostatic form is less than 1 kbar (0.1 GPa). The application of DFT-based total-energy calculations to the study of semiconductors properties under high pressure was reviewed in Ref. 69, showing that the phase stability, electronic, and dynamic properties of compounds under pressure are well describe by DFT.

Since the calculation of the disordered bcc phase is not possible with VASP code, we attempted to perform calculations for the bcc-like monoclinic $C2/m$ structure proposed in Ref. 41. Furthermore, since the thermodynamic phase transition between two structures occurs when the Gibbs free energy G is the same for both phases, we obtained G for the different phases using a quasiharmonic Debye model.[70] This model allowed us to obtain G at room temperature from calculations performed for $T = 0$K to discuss the relative stability of the different phases proposed in the present work.

To test our calculations, we show in Table I the calculated lattice parameters in the different phases of Bi_2Se_3 at different pressures. For comparison, we show in Table I other available theoretical calculations and experimental results. As far as the R-3m phase is concerned, our calculated lattice parameters are in relatively good agreement with experimental values from Ref. 5 and are similar to those calculated in Ref. 59 with GGA–Perdew-Burke-Ernzerhof (PBE), both with and without considering the SO coupling. In addition, we give the calculated lattice parameters of Bi_2Se_3 in the $C2/m$ and $C2/c$ structures at 13.5 and 25.5 GPa, respectively, for comparison with experimental data. In Table I, the a and b parameters of the $C2/m$ and $C2/c$ structures at 13.5 and 25.5 GPa for Bi_2Se_3 are similar to those reported by Zhu *et al.* for Bi_2Te_3[41]; however, the c lattice parameter and β angle for monoclinic $C2/m$ and $C2/c$ structures differ from those obtained by Zhu *et al.* The reason is that the results of our *ab initio* calculations are given in the standard setting for the monoclinic structures, in contrast with Ref. 41, for better comparison to future experiments, since many experimentalists use the standard setting.

We also performed lattice dynamics calculations of the phonon modes in the R-3m, $C2/m$, and $C2/c$ phases at the zone center (Γ point) of the BZ to confirm whether experimentally measured Raman scattering of the high-pressure phases of Bi_2Se_3 can be explained with the proposed structures. Our theoretical results enable us to assign the Raman modes observed for the different phases of Bi_2Se_3. Furthermore, the calculations provide information about the symmetry of the modes and polarization vectors that is not readily accessible

in the present experiment. Highly converged results on forces are required for the calculation of the dynamic matrix. We use the direct force constant approach (or supercell method).[71] The construction of the dynamic matrix at the Γ point of the BZ is particularly simple and involves separate calculations of the forces in which a fixed displacement from the equilibrium configuration of the atoms within the *primitive* unit cell is considered. Symmetry aids by reducing the number of such independent displacements, thus reducing the computational effort in the study of the analyzed structures considered in this work. Diagonalization of the dynamic matrix provides both the frequencies of the normal modes and their polarization vectors. It allows to us to identify the irreducible representation and the character of the phonons modes at the Γ point. In this work, we provide and discuss the calculated frequencies and pressure coefficients of the Raman-active modes for the three calculated phases of Bi_2Se_3. The theoretical results obtained for infrared (IR)–active modes for the three calculated phases of Bi_2Se_3 are given as Supplementary Material for this article.[72]

As we commented in our previous papers,[50,51] we also checked the effect of the SO coupling in the structural stability and the phonon frequencies of the R-3m phase of Bi_2Se_3. We found that the effect of the SO coupling is very small and did not affect significantly our results (small differences of 1–3 cm^{-1} in the phonon frequencies at the Γ point). However, calculations for the phases with a lot of atoms in the unit cell are more time consuming. Therefore, the theoretical values corresponding to lattice dynamics calculations in the present paper do not include the SO coupling, except for those corresponding to the R-3m phase.

IV. RESULTS AND DISCUSSION

A. XRD in Bi_2Se_3

Figure 1 shows the x-ray powder diffraction data of Bi_2Se_3 up to 20 GPa. The room pressure x-ray pattern of α-Bi_2Se_3 was indexed with a rhombohedral structure (R-3m, SG 166) and with lattice parameters $a = 4.123(1)$ Å, $c = 28.486(1)$ Å, and $V_0 = 419.3(2)$ Å^3. These values are slightly smaller than those from Nakajima *et al.* ($a = 4.143$ Å, $c = 28.636$ Å, and $V_0 = 425.673$ Å^3).[5] The initial rhombohedral structure is stable up to 9.7 GPa, where a phase transition occurs. The onset on the phase transition is placed at 9.7 GPa, so the two phases (the initial and the high-pressure ones) coexisting up to at least 12 GPa. As can be seen in Fig. 1, the phase transition is fully reversible after increasing pressure to 20 GPa and releasing pressure to room pressure. We indexed the diffraction patterns between 10 and 20 GPa as corresponding to the monoclinic $C2/m$ phase. Figure 2 shows a full Rietveld refinement with the $C2/m$ structure of the XRD pattern obtained at 13.5 GPa and carried out using the FullProf program, along with the obtained residuals. Lattice parameters and atomic positions obtained from the Rietveld refinement are shown in Table II.

Figures 3 and 4 show the experimental and theoretical pressure dependence of the volume and lattice parameters in both α-Bi_2Se_3 and β-Bi_2Se_3, respectively, while the inset of Fig. 4(a) shows the c/a ratio vs pressure dependence. Our measured pressure dependence of the volume, lattice parameters, and c/a ratio agree nicely with those predicted

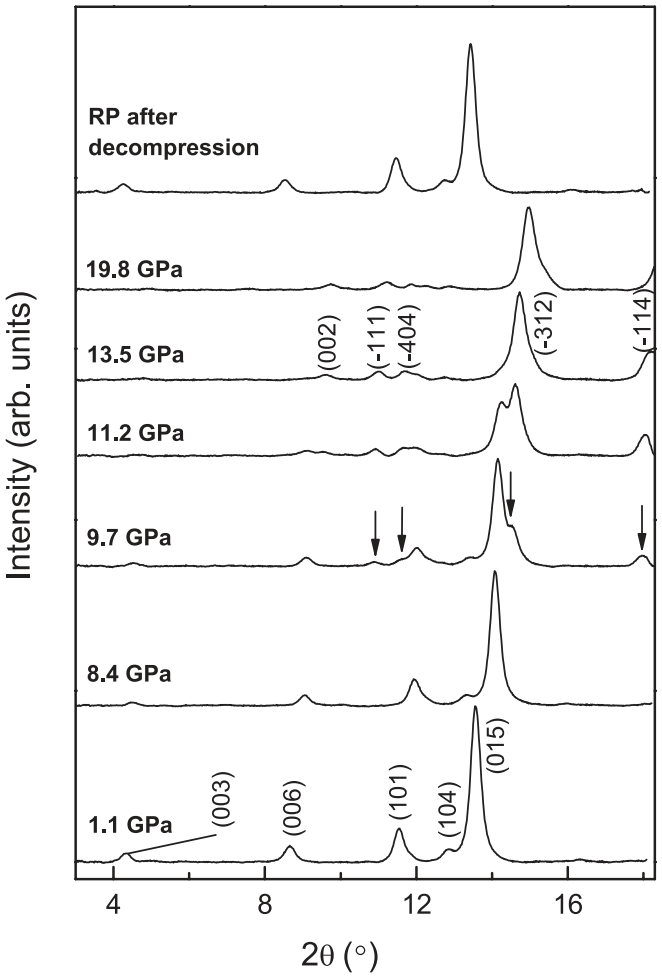

FIG. 1. Selected x-ray powder diffraction patterns of Bi_2Se_3 at different pressures showing the low- and high-pressure phases of Bi_2Se_3. Backgrounds were subtracted. Arrows indicate the appearance of new diffraction peaks corresponding to the high-pressure phase (β-Bi_2Se_3). The spectrum at room pressure (RP) after releasing pressure from 20 GPa is also shown.

by total-energy *ab initio* calculations (solid lines in Figs. 3 and 4). Fit of the volume vs pressure in α-Bi_2Se_3 to a Birch-Murnaghan equation of state (BM-EOS) yields the following data for the volume, bulk modulus, and its pressure derivative at room pressure: $V_0 = 420(1)$ Å^3, $B_0 = 53(8)$ GPa, and $B_0' = 2.9(2)$, respectively. Similarly, fit of the volume vs pressure in β-Bi_2Se_3 to a BM-EOS yields following data

TABLE II. Rietveld-refined fractional coordinates corresponding to the high-pressure phase of Bi_2Se_3 at 13.5 GPa. The structure is monoclinic ($C2/m$ SG) with lattice parameters $a = 14.007(6)$ Å, $b = 3.829(1)$ Å, $c = 8.471(6)$ Å, and $\beta = 88.31(4)$.

Atom	Site	x	y	z
Bi1	4i	0.023(1)	0	0.194(1)
Bi2	4i	0.234(1)	0	0.221(1)
Se1	4i	0.169(2)	0	0.386(3)
Se2	4i	0.416(2)	0	0.413(4)
Se3	4i	0.359(2)	0	0.000(4)

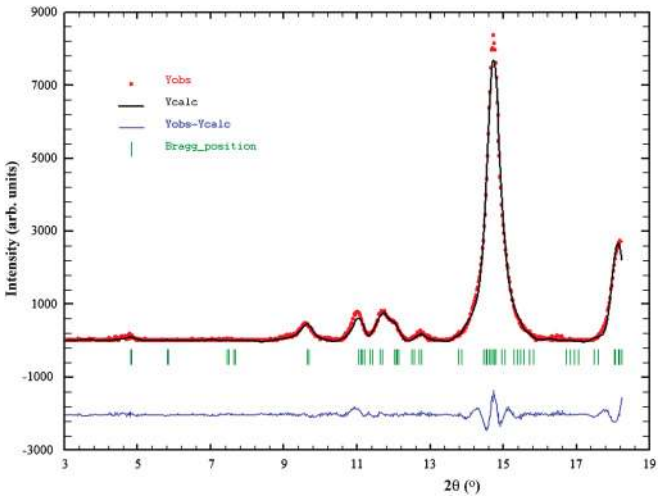

FIG. 2. (Color online) Observed (solid circles), calculated, and difference (solid lines) XRD profiles of the high-pressure phase of Bi_2Se_3 at 13.5 GPa. Vertical markers indicate Bragg reflections. The R_{Bragg}, R_{wp}, and R_p residuals are 3.36%, 16.4%, and 12.5%, respectively. Lattice parameters and atomic positions are collected in Table II.

for the volume, bulk modulus, and its pressure derivative at room pressure: $V_0 = 529(2)$ Å^3, $B_0 = 66(3)$ GPa, and $B_0' = 4.5$ (fixed), respectively. These results are compared to our theoretical results and other results published in the literature in Table I. We also studied the axial compressibilities for α-Bi_2Se_3 by fitting to a BM-EOS the volume of a pseudocubic cell vs pressure, where the volume of this pseudocubic cell is calculated for axes a and c as $V_a = a^3$ and $V_c = c^3$, respectively.[73] The obtained results for the bulk modulus and its pressure derivative at room pressure are, for

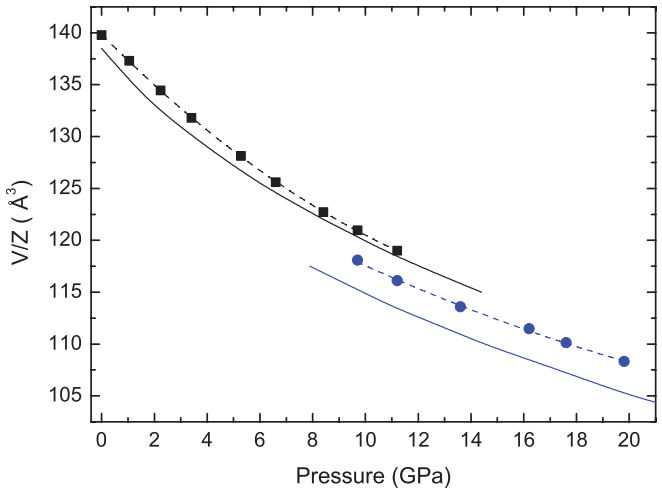

FIG. 3. (Color online) Pressure dependence of the unit cell volume for both the low-pressure (R-3m) and the high-pressure ($C2/m$) phases of Bi_2Se_3 under compression. Experimental volumes per unit formula for the low- and high-pressure phases as a function of pressure are represented by solid squares and circles, respectively. Dashed and solid lines show the fit to a BM-EOS for experimental and theoretical data, respectively. Error bars for experimental data are smaller than experimental data points.

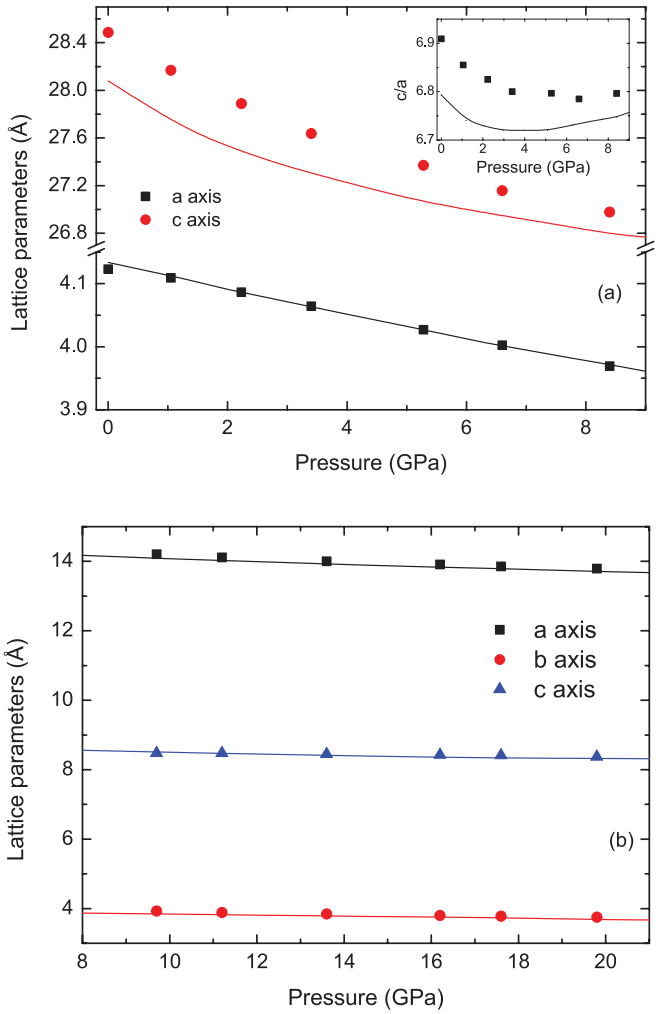

FIG. 4. (Color online) (a) Pressure dependence of the lattice parameters for the low pressure (R-3m). The inset shows the c/a ratio vs pressure dependence. (b) Pressure dependence of the lattice parameters for the high-pressure ($C2/m$) phases of Bi_2Se_3. Experimental and theoretical data are represented by symbols and lines, respectively. Error bars for experimental data are smaller than experimental data points.

the c axis, $B_0 = 26(2)$ GPa and $B_0' = 9(1)$ and, for a axis, $B_0 = 62(2)$ GPa and $B_0' = 4$(fixed). As can be observed, the c axis is more compressible than the a axis.

A pressure-induced ETT occurs in α-Bi_2Te_3 and α-Sb_2Te_3, whose structure is the same as that of α-Bi_2Se_3.[36,38,39,42,43] Recently, it was observed that the ETT in α-Bi_2Te_3 leads to a change in compressibility around 3.2 GPa without a change in volume but with a pronounced change in the c/a ratio behavior at pressures below and above the ETT.[39,43] We observe similar changes in the compressibility and in the c/a ratio around 5 GPa (~4 GPa in theoretical calculations) in Bi_2Se_3 that suggest the presence of an ETT in this compound near 5 GPa. To confirm whether α-Bi_2Se_3 undergoes an ETT, we performed a more accurate analysis of the volume and lattice parameters vs pressure up to 8 GPa, as plotted in Figs. 3 and 4. In this sense, we performed a linearization of the BM-EOS vs the Eulerian strain:

$$H = B_0 + \tfrac{3}{2}B_0(B_0' - 4)f_E, \quad (1)$$

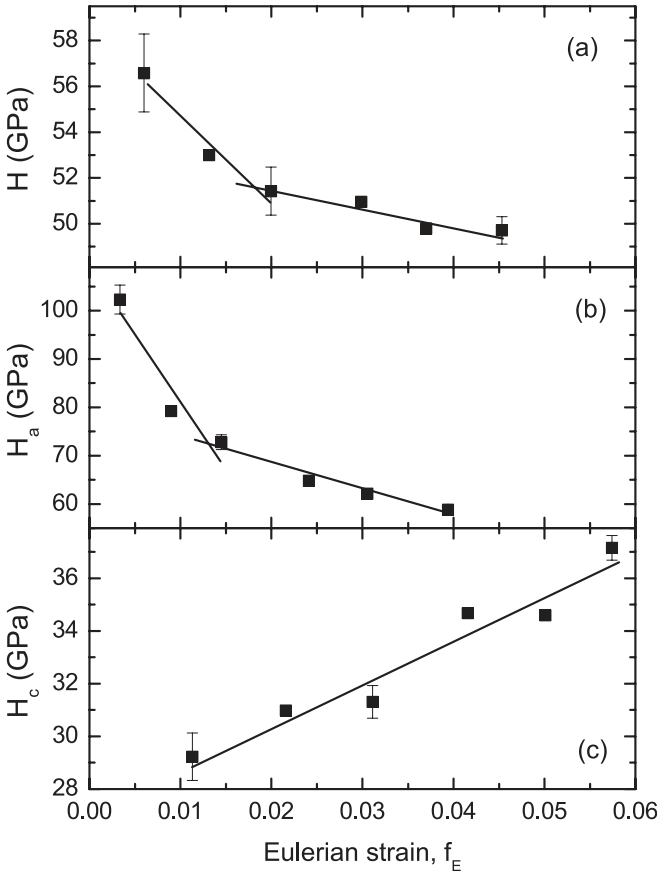

FIG. 5. Dependence of the reduced pressure (a) H, (b) H_a, and (c) H_c vs the Eulerian strain f_E. Straight lines represent linear fits to the data points in two different regions for (a) and (b) and in the whole region for (c).

where

$$H = \frac{P}{3 \cdot f_E \cdot (1 + 2 \cdot f_E)^{5/2}} \tag{2}$$

is the reduced pressure and

$$f_E = \frac{(X^2 - 1)}{2} \tag{3}$$

is the Eulerian strain, with

$$X = \left(\frac{V_0}{V}\right)^{1/3}. \tag{4}$$

Plotted in this way, the reduced pressure H vs the Eulerian strain f_E should be linear for any stable compound. Furthermore, taking into account Eq. (1), we can obtain the bulk modulus of the compound at zero pressure B_0 and its pressure derivative B_0'. Figure 5(a) shows the $H(f_E)$ plot for the volume. That plot shows a rather clear change in the slope of H around 3.4 GPa, suggesting the presence of an ETT near 3.4 GPa. The obtained values for B_0 and B_0' using Eq. (1) from the volume data before and after 3.4 GPa are $B_0 = 59(1)$ GPa, $B_0' = -0.2(1)$ and $B_0 = 53(1)$ GPa, $B_0' = 3.1(8)$, respectively. Figures 5(b) and 5(c) shows the $H(f_E)$ plot for the a (H_a) and c (H_c) axes, respectively. To obtain the reduced pressure for the a and c axes, we used Eqs. (2)–(4) but with $X_a = a_0/a$ and $X_c = c_0/c$ for the a and c axes, respectively. Analyzing the pressure dependence of H_a and H_c in Fig. 5, the change of the slope of H is related to the change found in H_a, while H_c shows no change in compressibility between 0 and 8 GPa. For the case of the a lattice parameter, the values for B_0 and B_0' obtained using Eq. (1) from the a-axis data before and after the 2.2 GPa are $B_0 = 109(9)$ GPa, $B_0' = -12(5)$ and $B_0 = 80(2)$ GPa, $B_0' = -0.6(1)$, respectively. In some cases, a negative value for B_0' is obtained, which has no physical meaning because we expect the B_0 parameter to increase as pressure increases. The straight lines in Fig. 5 are tentatively drawn, and we would have needed more experimental points to describe the change in the slope with less uncertainty. Therefore, further experiments in a synchrotron source are needed to obtain more accurate values for the B_0 and B_0' parameters both before and after the pressure at which the ETT occurs. For the case of the c axis where no change in slope is found, the values for B_0 and B_0' calculated from Eq. (1) are $B_0 = 27.1(8)$ GPa and $B_0' = 8.0(1.2)$. The latter values are in good agreement with those obtained from the BM-EOS fit. Therefore, the analysis of the reduced pressures for a and V as a function of the Eulerian strain gives us a qualitative picture that supports the presence of the ETT due to the change of the slope in both figures. This confirms that the change of the c/a ratio with pressure is a good indicator of the ETT since it is caused by the anomalous behavior of a as a function of pressure, which in turn results in a change in the compressibility at the ETT.

In conclusion, our XRD measurements reveal the occurrence of an ETT in α-Bi_2Se_3 which is related to a change in the layer compressibility as it occurs in α-Bi_2Te_3.[43] The presence of an ETT in α-Bi_2Se_3 is in agreement with previously reported electric resistivity measurements.[28] However, we found a phase transition above 9.7 GPa in α-Bi_2Se_3 that seems to have the $C2/m$ structure, i.e., the same structure found in α-Bi_2Te_3 above 9 GPa.[41]

B. Raman scattering of α-Bi_2Se_3

The rhombohedral structure of Bi_2Se_3 is centrosymmetric, and group theory allows 10 zone-center modes that decompose in the irreducible representations as follows:[53,54]

$$\Gamma_{10} = 2A_{1g} + 3A_{2u} + 2E_g + 3E_u. \tag{5}$$

The two acoustic branches come from one A_{2u} and a doubly degenerated E_u mode, while the rest correspond to optic modes. Gerade (g) modes are Raman active, while ungerade (u) modes are IR active. Therefore, there are four Raman-active modes ($2A_{1g} + 2E_g$) and four IR-active modes ($2A_{2u} + 2E_u$). The E_g modes correspond to atomic vibrations in the plane of the layers, while the A_{1g} modes correspond to vibrations along the c axis perpendicular to the layers.[53,54]

Figure 6 shows the experimental Raman spectra of rhombohedral Bi_2Se_3 at different pressures up to 8.6 GPa. We observed and followed under pressure three of the four Raman-active modes. The E_g mode calculated to be close to 40 cm^{-1} was not observed in our experiments or in previous Raman scattering measurements at room pressure in bulk material;[6,54] however, this mode was observed recently in nanoplatelets.[56] Figure 7(a) shows the experimental pressure dependence of the frequencies of the three first-order Raman modes measured in α-Bi_2Se_3 that are compared with the pressure dependence of

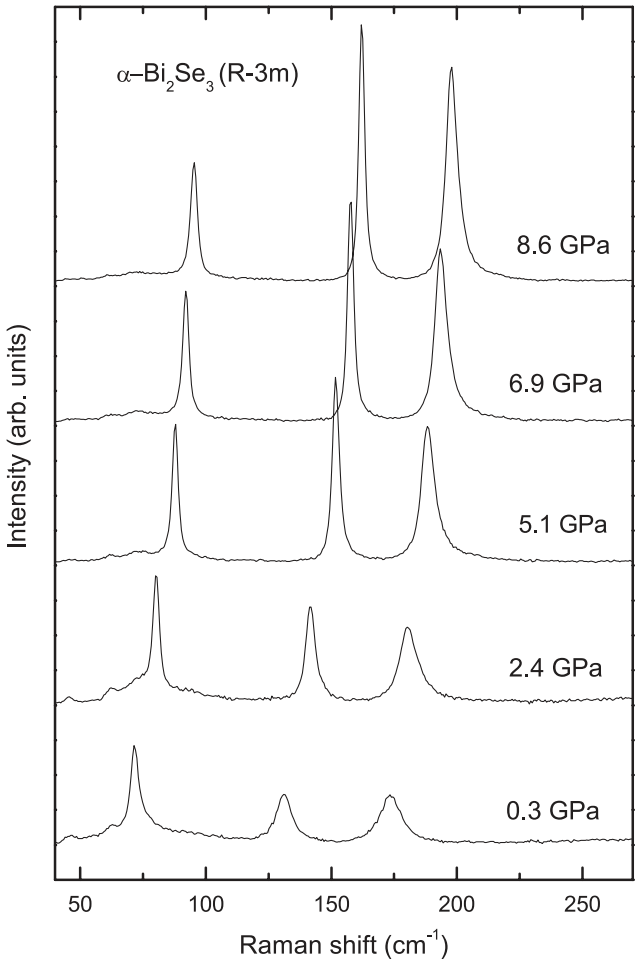

FIG. 6. Experimental Raman spectra of α-Bi_2Se_3 at pressures between 1 atm and 8.6 GPa.

our calculated theoretical frequencies. Table III summarizes our experimental and theoretical first-order Raman-mode frequencies and pressure coefficients in the rhombohedral phase. Our experimental frequencies at room pressure are in good agreement with those already measured in Refs. 54 and 56 (Table III). In addition, our theoretical frequencies at room pressure are also in good agreement with those reported in Ref. 59 both with and without SO coupling (Table III).

In Fig. 7(a), all measured Raman modes exhibit hardening with increasing pressure. The experimental values of the frequencies and pressure coefficients are in a general good agreement with our theoretical calculations (Table III); however, a decrease of the pressure coefficient of the A_{1g}^1 and E_g^2 modes occurs around 5 GPa [dashed lines in Fig. 7(a)]. Anomalies in the phonon spectrum are also expected for materials undergoing an ETT[45,46] and were observed in a number of materials,[47,48] as well as in $Sb_{1.5}Bi_{0.5}Te_3$.[38] Therefore, we attributed the less positive pressure coefficient of these two Raman modes to a pressure-induced ETT. In previous studies in Sb_2Te_3 and Bi_2Te_3 under pressure, we experimentally measured a change in the pressure coefficient of the frequency of several modes.[50,51] To support our hypothesis, we plot in Fig. 7(b) the pressure dependence of the linewidth of the three measured Raman modes. Curiously, the full width at half maximum (FWHM) changes its slope around 5 GPa, thus confirming an anomaly related to the ETT as was evidenced in Sb_2Te_3 and Bi_2Te_3 under pressure.[50,51] Therefore, our results of the pressure dependence of the frequency and the linewidth support the observation of the ETT around 5 GPa in α-Bi_2Se_3, similar to the case of α-Sb_2Te_3[50] and α-Bi_2Te_3.[51]

The large linewidth of the first-order Raman modes at ambient pressure can only be accounted for by a rather strong phonon–phonon interaction (i.e., anharmonic decay) causing a decrease of the phonon lifetimes. This is likely due to the coincidence of the first-order Raman-mode frequencies with a high density of the two-phonon (sum) density of states. In this sense, the decrease of the linewidth of the Raman-active modes with increasing pressure can be understood by the separation of the first-order Raman-active modes with respect to the frequency of the high density of the two-phonon (sum) density of states due to the larger pressure coefficient of the

TABLE III. Experimental (exp.) room temperature Raman-mode frequencies and pressure coefficients observed in α-Bi_2Se_3 at both $P_0 = 1$ atm and 5.0 GPa, as obtained from fits to the data using $\omega(P) = \omega(P_0) + a_1 \times (P - P_0)$. Theoretical (th.) values calculated at room pressure are shown for comparison, as well as theoretical and experimental data from Refs. 54, 56, and 59.

Mode	$\omega(P = P_0)$ (exp.) (cm^{-1})	a_1 (exp.) (cm^{-1}/GPa)	$\omega(P = 1$ atm) (th.) (cm^{-1})	a_1 (th.) (cm^{-1}/GPa)	$\omega(P = 1$ atm) (exp.) (cm^{-1})	$\omega(P = 1$ atm) (th.) (cm^{-1})	$\omega(P = 1$ atm) (th.) (cm^{-1})
E_g^1			41.8	1.47	37	42.1	38.9
A_{1g}^1	72.2(5)[b]	3.2(1)[b]	74.4	2.53	72	74.6	63.85
	88.3(3)[c]	1.98(1)[c]					
E_g^2	131.4(6)[b]	4.1(1)[b]	136.2	3.13	131	138.9	124.0
	153.5(3)[c]	2.3(3)[c]					
A_{1g}^2	174(1)[b]	2.92(2)[b]	174.3	2.68	174	179.5	166.4
	188.3(7)[c]	2.65(7)[c]					
Refs.	[a]	[a]	[a]	[a]	54 and 56	59[d]	59[e]

[a]This work.
[b]Calculated at room pressure ($P_0 = 1$ atm).
[c]Calculated at $P_0 = 5.0$ GPa.
[d]GGA calculations without SO coupling.
[e]GGA calculations with SO coupling.

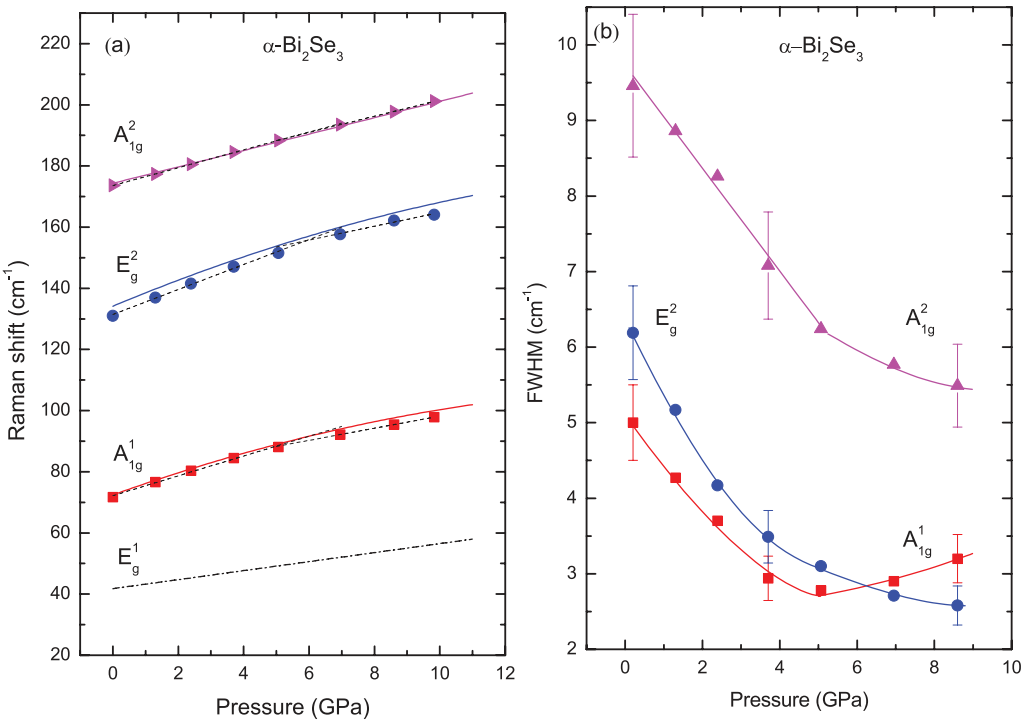

FIG. 7. (Color online) (a) Experimental pressure dependence of the Raman-mode frequencies in α-Bi_2Se_3. Solid and dashed-dotted curves represent *ab initio* calculated mode frequencies of modes observed and not observed, respectively, in our measurements. Dashed lines represent different behavior of the experimental Raman mode with pressure. Error bars for experimental data are smaller than or equal to experimental data points. (b) Experimental pressure dependence of the FWHM of the Raman modes. Solid lines represent two different behaviors of the FWHM with pressure.

first-order Raman modes than the sum of two-phonon states, which usually involves acoustic modes with very small or even negative pressure coefficients.[74]

Similar to the case of α-Sb_2Te_3[50] and α-Bi_2Te_3,[51] our results for α-Bi_2Se_3 show that the high-frequency A_{1g} mode is almost not altered near the ETT, in good agreement with our calculations; however, we noted a clear change of the pressure coefficient of the frequency for both the lower A_{1g} and the higher-frequency E_g modes. Since A_{1g} modes are polarized in the direction perpendicular to the layers while the E_g modes are polarized along the layers, our observation of a less positive pressure coefficient of both types of modes in Bi_2Se_3 could suggest that the ETT in Bi_2Se_3 is related to a change of the structural compressibility of both the direction perpendicular to the layers and the direction along the layers. This seems not to be in agreement with our results of XRD or with those of Polian *et al.* for Bi_2Te_3,[43] where the ETT only affects the compressibility of the plane of the layers. In this sense, the change of pressure coefficient around 5 GPa in Bi_2Se_3 is bigger for the E_g mode than for the A_{1g} modes, which is in good agreement with the larger change in compressibility along the layers than in the direction perpendicular to the layers. However, the same is not true in the case of Bi_2Te_3, where the change of the pressure coefficient at 4 GPa in Bi_2Te_3 is bigger for the A_{1g} mode than for the E_g mode.[51] Consequently, more work is needed to understand the mechanism of the ETT in this material.

It is timely to conclude this section by comparing the Raman-mode frequencies and their pressure coefficients in α-Bi_2Se_3 with those of α-Sb_2Te_3[50] and α-Bi_2Te_3[51] and with other layered materials. In chalcogenide laminar materials, the two lowest-frequency E and A modes are usually related to shear vibrations between adjacent layers along the *a*–*b* plane and to vibrations of one layer against the others along the *c* axis, respectively. Some authors have commented that the E mode displays the smallest pressure coefficient, which is consistent with the weak bending force constant between the interlayer distances (in our case, Se-Se distances), while the A mode displays the largest pressure coefficient due to the extraordinary increase of the stretching force constant between the interlayer distances.[50,51] For example, the E and A modes with frequencies around 40 (60) cm^{-1} and 116 (133) cm^{-1} in InSe (GaSe), respectively, have pressure coefficients of 0.68 (0.85) cm^{-1}/GPa and 5.41 (5.78) cm^{-1}/GPa.[75,76] In α-Bi_2Se_3, our theoretical calculations show that the two lowest-frequency A_{1g} and E_g modes have rather similar pressure coefficients in comparison to other layered chalcogenides like InSe and GaSe. This result is consistent with smaller anisotropy in the intralayer and interlayer properties of Bi_2Se_3 than in InSe and GaSe. We arrived at a similar conclusion in our studies of α-Sb_2Te_3[50] and α-Bi_2Te_3,[51] and we attributed it to the stronger interlayer interaction occurring in Bi_2Se_3, Bi_2Te_3, and Sb_2Te_3 favored by the SO coupling, which is absent in other laminar chalcogenides, like InSe and GaSe.

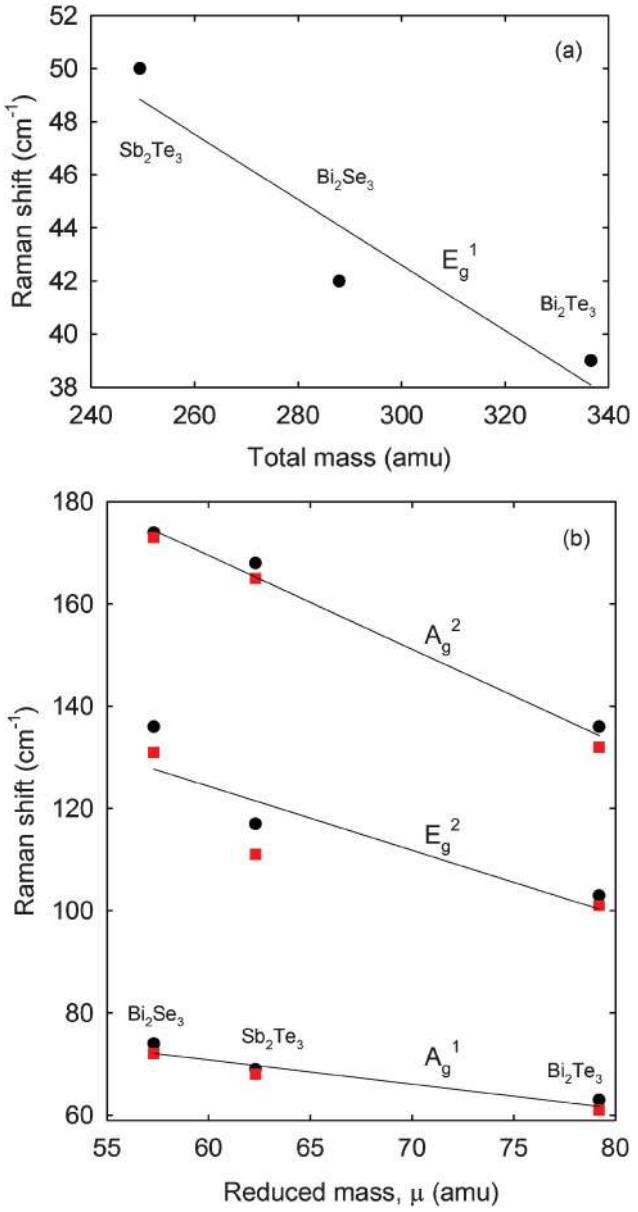

FIG. 8. (Color online) Experimental (squares) and theoretical (circles) frequencies of the Raman-active modes of α-Bi_2Se_3, α-Bi_2Te_3, and α-Sb_2Te_3 as a function of (a) the total mass and (b) the reduced mass of the AX (A = Sb,Bi; X = Se,Te) molecule. Error bars for experimental data are smaller than or equal to experimental data points.

Finally, regarding the Raman modes of the rhombohedral structure in Bi_2Se_3, Bi_2Te_3, and Sb_2Te_3, we plot in Fig. 8 the frequencies of the Raman-active modes in the three compounds as a function of the total mass of the (Bi,Sb)-(Se,Te) molecule and its reduced mass. The theoretical values obtained for the lowest-frequency E_g^1 mode scale with the total mass of the molecule ($m_T = m_C + m_A$; C = cation, A = anion), so both anion and cation have a considerable contribution to this mode, especially the cation in Bi_2Se_3 and Bi_2Te_3. Contrarily, the experimental and theoretical frequencies of the other three modes scale with the reduced mass μ of the molecule ($1/\mu = 1/m_C + 1/m_A$). This especially true for the A_{1g} modes, and it means that in these modes the anion movement has a slightly larger contribution than the cation movement. Regarding the pressure coefficients of the Raman-active modes, the E_g^1 mode has a value around 2 cm^{-1}/GPa in the three compounds, being larger for Sb_2Te_3 and smaller for Bi_2Se_3. However, the A_{1g}^1 mode has values between 3.2 and 4.5 cm^{-1}/GPa in the three compounds, again being larger for Sb_2Te_3 and smaller for Bi_2Se_3. Our results show that the difference of pressure coefficient between the interlayer mode (A_{1g}^1) and the intralayer mode (E_g^1) is larger for Sb_2Te_3 and smaller for Bi_2Se_3, and this result suggests that, despite being the compound with the smaller SO coupling, Bi_2Se_3 is the compound showing smaller anisotropy in the interlayer and intralayer properties. However, the smaller pressure coefficients of the lower-frequency modes in Bi_2Se_3 than in Bi_2Te_3 and Sb_2Te_3, which are more influenced by interlayer vibrations, suggest that the interlayer bonds of the van der Waals type tend to harden at a smallest rate with pressure in Bi_2Se_3 compared to that in the other two compounds; i.e., the anisotropy in the properties along the layers and perpendicular to the layers tends to disappear more slowly with increasing pressure in Bi_2Se_3 than in Bi_2Te_3 and Sb_2Te_3. However, the experimental pressure coefficients of the E_g^2 and the A_{1g}^2 modes are rather similar in the three compounds. In particular, for the A_{1g}^2 mode, it is the same (2.9 cm^{-1}/GPa) for the three compounds, although our calculations suggest that it should be somewhat smaller for Sb_2Te_3. Since these two high-frequency modes are mainly related to intralayer vibrations, their similar pressure coefficients suggest a rather similar covalent nature of the intralayer bonds in the three compounds.

C. Raman scattering of β-Bi_2Se_3

It has been demonstrated in a joint experimental and theoretical work that α-Bi_2Te_3 undergoes a phase transition around 7.5 GPa toward a β-Bi_2Te_3 phase with monoclinic $C2/m$ structure.[41] Figure 9(a) shows the experimental Raman spectra of β-Bi_2Se_3 at different pressures from 10 to 19 GPa, which according to our x-ray powder diffraction measurements correspond to Raman active modes of the $C2/m$ structure. In the monoclinic $C2/m$ structure, all Bi and Se atoms occupy 4i Wyckoff sites. Therefore, group theoretical considerations predict 30 vibrational modes with the following representation:

$$\Gamma_{30} = (10A_g + 10B_u) + (5B_g + 5A_u). \quad (6)$$

From them, one A_u and two B_u are the acoustic phonons and the rest are optical phonons. Consequently, we expect 15 zone-center Raman-active ($10A_g + 5B_g$) modes for the $C2/m$ phase. For comparison we marked in Fig. 9(a) the calculated Raman-mode frequencies for this phase at 9.8 GPa to compare it with the Raman spectrum at 9.8 GPa. The frequencies of the experimental Raman modes agree reasonably with our calculations. Figure 9(b) shows the pressure dependence of the experimental and theoretical Raman-mode frequencies in β-Bi_2Se_3. There is consistent agreement between the experimental and theoretical Raman-mode frequencies and their pressure coefficients. Therefore, we can reasonably confirm that the β-Bi_2Se_3 phase has the monoclinic $C2/m$ structure already found in Bi_2Te_3 by means of XRD measurements.[41]

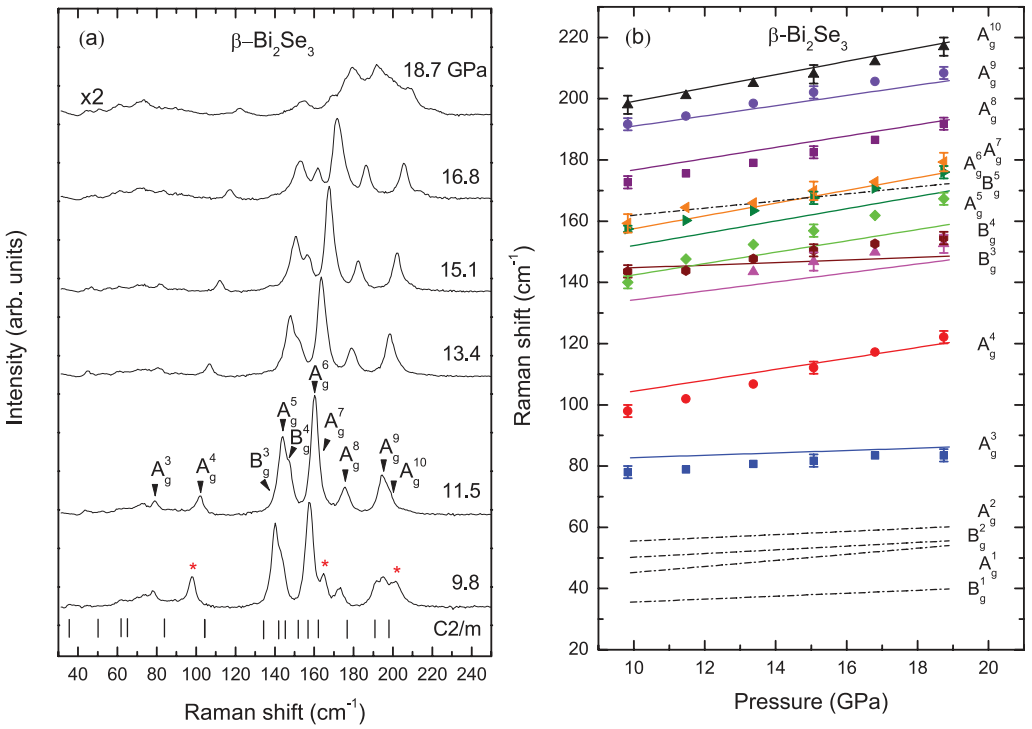

FIG. 9. (Color online) (a) Experimental Raman spectra of the high-pressure phase of β-Bi_2Se_3 at pressures between 9.8 and 18.7 GPa. Bottom marks indicate the calculated frequencies of the Raman-active modes in the β-Bi_2Se_3 phase at 9.8 GPa. Asterisks mark the Raman peaks remaining from the R-3m phase at 9.8 GPa. (b) Experimental pressure dependence of the Raman-mode frequencies in β-Bi_2Se_3. Solid and dashed-dotted curves represent *ab initio* calculated mode frequencies of modes observed and not observed, respectively, in our measurements.

Table IV summarizes the experimental and theoretical first-order Raman-mode frequencies and pressure coefficients at 9.8 GPa in β-Bi_2Se_3.

In our experiments, we have not observed the four lowest-frequency modes (A_g^1, B_g^1, A_g^2, and B_g^2), whose detection is difficult because they could be weak and their frequencies are below the cutting edge of our Raman edge filter for the LabRAM spectrometer. However, other weak low-frequency modes (A_g^3, A_g^4, and B_g^3) can be clearly followed under pressure. Finally, all highest-frequency modes are relatively intense and could be followed under pressure, with the only exception being the B_g^5 mode, which is likely masked by the stronger A_g^6 and A_g^7 modes [Figs. 9(a) and 9(b)]. The frequencies and pressure coefficients of these high-frequency modes are in good agreement with our calculations (Fig. 9(b) and Table IV), except for the pressure coefficients of the B_g^4 and A_g^5 modes. These results support our assignment of β-Bi_2Se_3 to the $C2/m$ phase. A decomposition of the Raman spectrum of the β-Bi_2Se_3 phase at 13.5 GPa into Voigt profiles can be observed in Fig. 1 in the Supplementary Material.[72]

Finally, we want to comment on the Bi coordination of β-Bi_2Se_3. At the R-3m–to–$C2/m$ phase transition pressure between 10 and 12 GPa, the highest-frequency mode of β-Bi_2Se_3 has a smaller frequency (198 cm^{-1}) than the highest-frequency mode of α-Bi_2Se_3 (203 cm^{-1}). This decrease in frequency of the highest-frequency mode, usually related to stretching Bi-Se vibrations, suggests an increase in the Bi-Se distance related to an increase of the Bi coordination from sixfold in α-Bi_2Se_3 to sevenfold in β-Bi_2Se_3. This result is in good agreement with the recently observed increase of the Bi coordination on going from α-Bi_2Te_3 to β-Bi_2Te_3[41,51]

TABLE IV. Experimental (exp.) Raman-mode frequencies and pressure coefficients observed in β-Bi_2Se_3 at room temperature at $P_0 = 9.8$ GPa, as obtained from fits using $\omega(P) = \omega(P_0) + a_1 \times (P - P_0)$. Theoretical (th.) *ab initio* values for the frequencies and pressure coefficients at 9.8 GPa are shown for comparison.

Mode	$\omega(P_0)$ (exp.) (cm^{-1})	a_1 (exp.) (cm^{-1}/GPa)	$\omega(P_0)$ (th.) (cm^{-1})	a_1 (th.) (cm^{-1}/GPa)
B_g^1			35.5	0.48
A_g^1			45.0	0.99
B_g^2			50.1	0.61
A_g^2			55.4	0.52
A_g^3	78(2)	0.68(7)	82.7	0.39
A_g^4	98(2)	2.76(5)	104.1	1.79
B_g^3	138(3)	1.69(4)	134.0	1.47
B_g^4	143(2)	1.3(1)	144.7	0.42
A_g^5	141(2)	3.0(1)	142.1	1.85
A_g^6	157(1)	2.07(9)	151.6	2.01
A_g^7	160(3)	2.1(2)	157.1	2.08
B_g^5			161.7	1.16
A_g^8	172(2)	2.12(9)	176.4	1.85
A_g^9	192(2)	1.95(6)	190.7	1.67
A_g^{10}	198(3)	2.11(7)	198.7	2.18

and of the Sb coordination on going from α-Sb_2Te_3 to β-Sb_2Te_3.[50]

D. Raman scattering of γ-Bi_2Se_3 and δ-Bi_2Se_3

It has been demonstrated in a joint experimental and theoretical work that β-Bi_2Te_3 undergoes a phase transition around 13.4 GPa toward a γ-Bi_2Te_3 phase with monoclinic $C2/c$ structure.[41] We observed that the Raman spectrum above 19.9 GPa is different from that of the $C2/m$ phase. Figure 10(a) shows the experimental Raman spectra of γ-Bi_2Se_3 at different pressures from 19.9 to 27.8 GPa. Furthermore, The Raman spectrum has almost disappeared at 27.8 GPa, suggesting a phase transition to a Raman-inactive phase above this pressure. In addition, on pressure release, we observed that the sample reverts to the original rhombohedral phase below 5 GPa after considerable hysteresis. The spectrum of the recovered sample in the rhombohedral phase at 1 atm after releasing pressure is shown as the last spectrum at the top of Fig. 10(a).

Group theoretical considerations predict 30 vibrational modes for the monoclinic $C2/c$ phase with the following representation:[50,51]

$$\Gamma_{30} = (7A_g + 7A_u) + (8B_g + 8B_u). \quad (7)$$

There are one A_u and two B_u acoustic modes and the rest are optical modes. Therefore, we expect 15 zone-center Raman-active modes ($7A_g + 8B_g$) for the $C2/c$ phase.

We marked in Fig. 10(a) the calculated Raman-mode frequencies for the $C2/c$ phase at 20 GPa to compare it with the Raman spectrum at 19.9 GPa. The frequencies of the experimental Raman modes agree reasonably with our calculations at this pressure, supporting the assignment of the γ-Bi_2Se_3 to the $C2/c$ phase. Furthermore, at 20 GPa, the highest-frequency mode of γ-Bi_2Se_3 has a smaller frequency (210 cm^{-1}) than the highest-frequency mode of β-Bi_2Se_3 ($\sim$220 cm^{-1}). This decrease in frequency of the highest-frequency mode again suggests an increase in the Bi-Se distance related to an increase of the Bi coordination from sevenfold in β-Bi_2Se_3 to eightfold in γ-Bi_2Se_3. This result is again in good agreement with the recently observed increase of the Bi coordination on going from β-Bi_2Te_3 to γ-Bi_2Te_3.[41,51]

Figure 10(b) shows the pressure dependence of the experimental and theoretical Raman-mode frequencies in γ-Bi_2Se_3. There is a reasonable agreement between the experimental and the theoretical Raman-mode frequencies and pressure coefficients for this phase. Therefore, we can reasonably suggest that the γ-Bi_2Se_3 phase has the monoclinic $C2/c$ structure already found by means of XRD measurements in Bi_2Te_3[41] and proposed as a high-pressure phase in Sb_2Te_3.[50] Table V summarizes the experimental and theoretical first-order Raman-mode frequencies and pressure coefficients in the γ-Bi_2Se_3 phase at 19.9 GPa.

In our experiments, we did not observe the four lowest-frequency modes (A_g^1, B_g^1, A_g^2, and B_g^2), whose detection is difficult because they could be weak in intensity and because their frequencies are below the cutting edge of the Raman edge filter of our spectrometer. Furthermore, they seem to be in a region where we observe several bands that we attribute

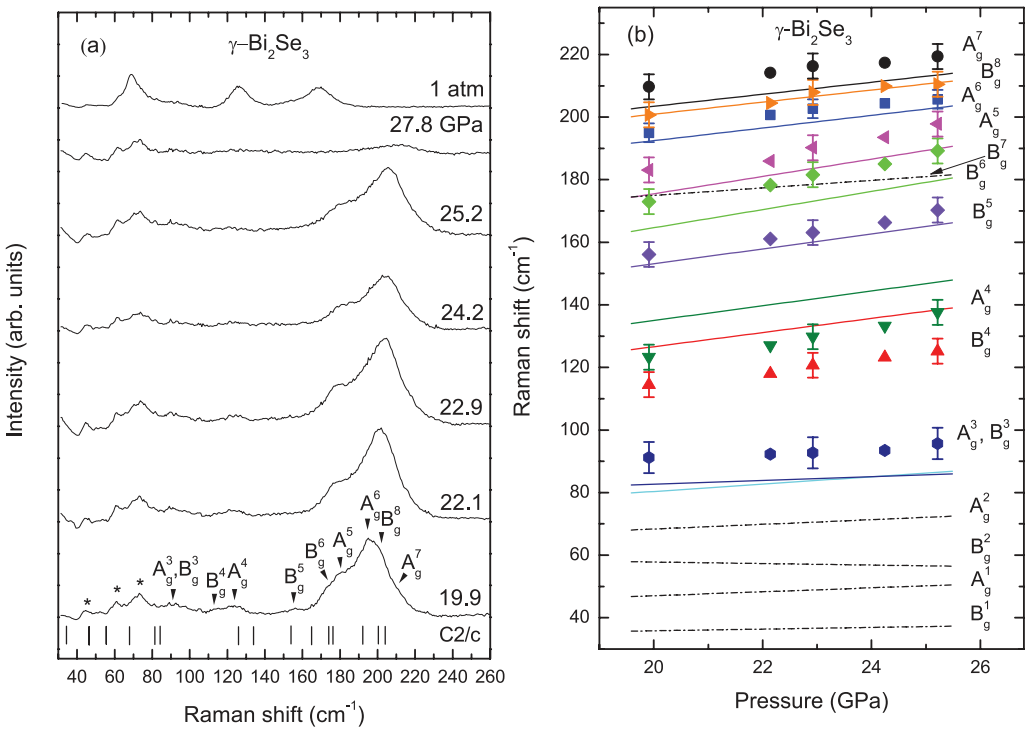

FIG. 10. (Color online) (a) Experimental Raman spectrum of γ-Bi_2Se_3 at pressures between 19.9 and 27.8 GPa and at ambient pressure after releasing pressure. The bottom marks indicate the calculated frequencies of the Raman-active modes in the γ-Bi_2Se_3 phase at 19.9 GPa. Asterisks are likely interferences from our edge filter (see text). (b) Experimental pressure dependence of the Raman-mode frequencies in γ-Bi_2Se_3. Solid and dashed-dotted curves represent *ab initio* calculated mode frequencies of modes observed and not observed, respectively, in our measurements.

TABLE V. Experimental (exp.) Raman-mode frequencies and pressure coefficients observed in γ-Bi_2Se_3 at room temperature at $P_0 = 19.9$ GPa, as obtained from fits using $\omega(P) = \omega(P_0) + a_1 \times (P - P_0)$. Theoretical (th.) *ab initio* values for the frequencies and pressure coefficients at 19.9 GPa are shown for comparison.

Mode	$\omega(P_0)$ (exp.) (cm^{-1})	a_1 (exp.) (cm^{-1}/GPa)	$\omega(P_0)$ (th.) (cm^{-1})	a_1 (th.) (cm^{-1}/GPa)
B_g^1			35.8	0.27
A_g^1			47.0	0.63
B_g^2			57.8	−0.24
A_g^2			68.3	0.74
B_g^3	91(5)	0.8(2)	80.2	1.18
A_g^3	91(5)	0.8(2)	82.6	0.61
B_g^4	114(4)	2.1(1)	126.4	2.26
A_g^4	122(4)	2.7(3)	134.8	2.36
B_g^5	156(4)	2.6(2)	152.9	2.38
B_g^6	172(4)	3.0(2)	164.3	2.90
A_g^5	182(4)	2.8(4)	175.2	2.76
B_g^7			174.8	1.20
A_g^6	196(3)	2.0(2)	192.3	2.02
B_g^8	201(4)	2.0(2)	200.7	1.93
A_g^7	210(4)	1.8(1)	203.3	1.92

to interferences from our edge filter [asterisks in Fig. 10(a)]. However, we attributed a broad band around 90 cm^{-1} to the weak modes A_g^3 and B_g^3. The other seven modes between 150 and 230 cm^{-1} form a broad band from which we decomposed six bands (see Fig. 2 in the supplementary material[72]). We have not evidenced the presence of the B_g^7 mode, whose predicted pressure behavior crosses the B_g^6 mode.

As we already commented, we detected a lack of Raman scattering signal above 27.8 GPa, suggesting a phase transition to a Raman inactive phase above that pressure. The lack of Raman scattering indicates that γ-Bi_2Se_3 undergoes a phase transition toward δ-Bi_2Se_3, and it suggests that the nature of the new phase could be the disordered bcc structure with the *Im*-3*m* SG recently found in Bi_2Te_3 above 14.4 GPa that dominates the XRD spectrum above 25 GPa.[40,41] The same disappearance of the Raman modes was recently observed in Sb_2Te_3 and attributed to a transition to a Raman-inactive phase, which could be a disordered bcc (but another phase, like a disordered body-centered cubic (fcc) or face-centered cubic (fcc), structure, cannot be excluded).[50] Our Raman measurements thus suggest that no phase transition to the monoclinic bcc-like $C2/m$ phase 9- or 10-fold Bi coordination occurs.[41] The main difference between the similar bcc-like $C2/m$ and disordered bcc (*Im*-3*m*) structures is that the bcc-like $C2/m$ phase is Raman active, with 12 Raman-active modes, while the *Im*-3*m* phase is Raman inactive. On the basis of our Raman measurements, we cannot assign δ-Bi_2Se_3 to the disordered bcc structure without ambiguity, because it is possible that the Raman scattering signal of the bcc-like $C2/m$ phase is very weak and we have not been able to measure it.

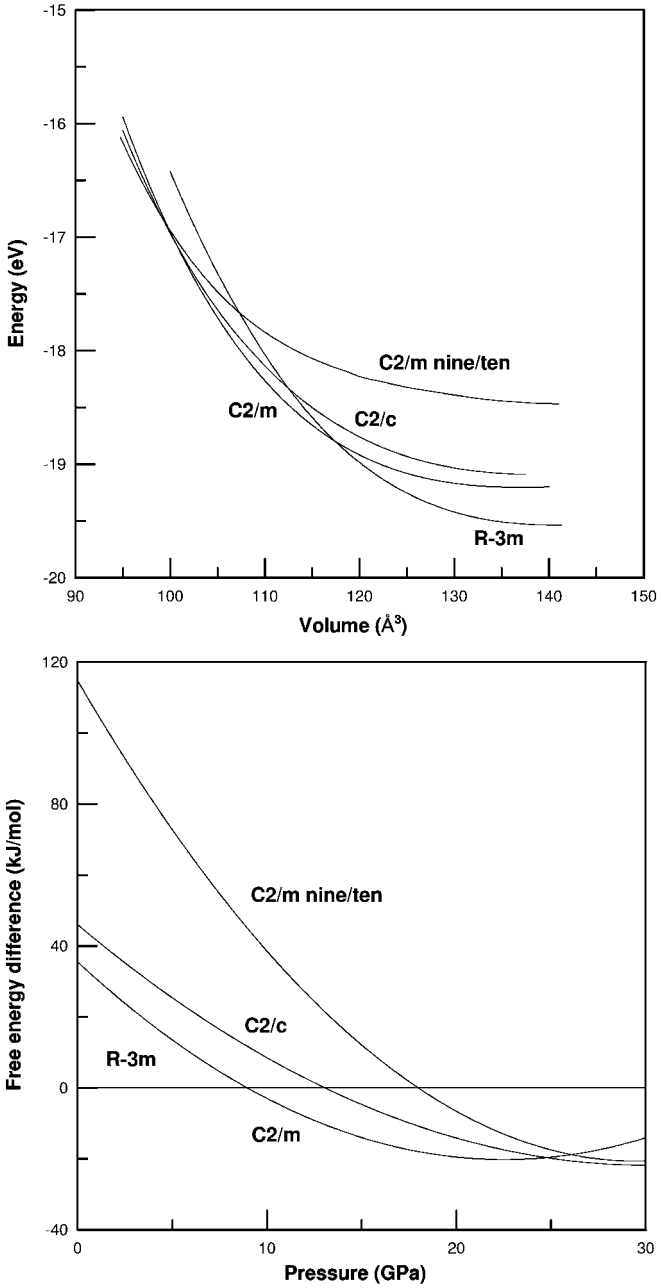

FIG. 11. Theoretical calculation of (a) energy vs volume and (b) Gibbs free energy difference vs pressure at 300K for the *R*-3*m*, $C2/m$, $C2/c$, and bcc-like $C2/m$ phases of Bi_2Se_3. Free energy of *R*-3*m* phase is taken as the reference in (b).

To study the structural stability of the different phases of Bi_2Se_3 and to support the previous assignments of the different high-pressure phases of Bi_2Se_3, we performed total-energy calculations for Bi_2Se_3 with the preceding proposed structures.[40,41] Figures 11(a) and 11(b) shows the energy vs volume and the Gibbs free energy difference at 300K vs pressure for the different phases calculated. In Fig. 11(a), the different phases observed in Bi_2Se_3 under pressure[41] cross one another at reduced volumes and therefore are candidates to be observed at different pressures. Therefore, our assignments of the peak frequencies in the preceding paragraphs to the

proposed phases are coherent. The only doubt is whether δ-Bi_2Se_3 is the bcc-like $C2/m$ 9- or 10-fold phase or the disordered bcc (Im-$3m$) phase. Our total-energy calculations support the phase transition from the $C2/c$ phase toward the bcc-like $C2/m$ phase. Unfortunately, we have not been able to made calculations for the disordered bcc phase with Im-$3m$ SG with the VASP code. Therefore, to ensure that these phases are consistent, we plot in Fig. 11(b) the pressure dependence of the Gibbs free energy difference at $T = 300$K for the different monoclinic phases with respect to the R-$3m$, which is taken as a reference. The calculated phase-transition pressure for the R-$3m$ to the $C2/m$ phase is 9 GPa, which compares well with the experimental value (9.7 GPa). The calculated phase-transition pressure for the $C2/m$ to the $C2/c$ phase is around 24.5 GPa, while the experimental value obtained from Raman measurements is around 19.9 GPa. Perhaps this disagreement is due to the presence of a slight uniaxial pressure in our Raman experiments, leading to a decrease of the phase transition pressure with respect to the value under truly hydrostatic conditions. Finally, regarding the last phase transition, our calculations of enthalpy show that the monoclinic bcc-like $C2/m$ 9- or 10-fold structure does not show a smaller enthalpy than the $C2/c$ phase. This means that in principle a phase transition from the $C2/c$ to the monoclinic bcc-like $C2/m$ phase cannot be observed at $T = 300$K. Furthermore, we calculated the phonons of the bcc-like $C2/m$ phase at pressures between 25 and 35 GPa and found that there are phonons with negative frequencies, which suggests that this phase is not really stable at those pressures. Therefore, we conclude that the δ-Bi_2Se_3 phase is most likely a disordered bcc phase with Im-$3m$ structure, as already found in Bi_2Te_3,[41] since it is expected that the Gibbs free energy of the disordered bcc structure is even lower than that of the bcc-like $C2/m$ phase. However, the attribution of the δ-Bi_2Se_3 phase to other Raman-inactive phases like a disordered fcc phase cannot be ruled out. Finally, it is possible that the phase transition from the $C2/c$ to the Raman inactive phase begins at much lower pressure than 28 GPa, as observed by XRD in Bi_2Te_3,[41] since Raman scattering cannot detect it because of the lack of Raman scattering of the latter phase. New XRD measurements at pressures above 20 GPa are needed to establish the onset of the phase transition to the δ-Bi_2Se_3 phase and to determine its crystalline structure.

V. CONCLUSIONS

We performed XRD and Raman scattering measurements at room temperature in Bi_2Se_3 up to 20 and 30 GPa, respectively, that were complemented with *ab initio* total-energy and lattice dynamics calculations. XRD measurements show that the layered-compound α-Bi_2Se_3 undergoes an ETT in the range 3–5 GPa, in which the bulk modulus changes as a consequence of the change of the layer compressibility. In addition, a phase transition toward a $C2/m$ structure (β phase) is observed between 10 and 12 GPa. However, Raman scattering measurements indicate that α-Bi_2Se_3 undergoes an ETT near 5 GPa and confirm the transition from the R-$3m$ to the $C2/m$ phase near 10 GPa, with an increase in coordination of Bi from 6 to 7. In addition, two other phase transitions were observed near 20 and 28 GPa, where Bi_2Se_3 is suggested to transform into a $C2/c$ structure (γ phase) and a disordered bcc structure (δ phase), respectively. The four structures here reported for Bi_2Se_3 are the same as those found previously in Bi_2Te_3[40,41,51] and Sb_2Te_3.[50] Our total-energy and lattice dynamics calculations fully support the experimental results here reported and allowed us to assign the symmetry of most of the Raman-active modes of the high-pressure phases. Finally, on fully releasing the pressure, the sample returns to the rhombohedral structure below 5 GPa, as occurs in the related materials Sb_2Te_3 and Bi_2Te_3.[50,51] We hope the present work will stimulate new measurements in Bi_2Se_3 under high pressure, especially to fully understand the mechanism of the ETT in the rhombohedral phase and the subtle effects on their structures and properties.

ACKNOWLEDGMENTS

This work was done under financial support from Spanish Ministry of Science and Innovation under Projects No. MAT2007-66129, No. MAT2010-21270-C04-03/04, and No. CSD-2007-00045 and from the Valencian government under Project No. Prometeo/2011-035. It is also supported by the Ministry of Education, Youth and Sports of the Czech Republic Project No. MSM 0021627501. E.P.G. acknowledges the financial support of the Spanish Ministry of Education. Supercomputer time was provided by the Red Española de Supercomputación and the MALTA cluster.

*rovilap@fis.upv.es

[1] G. J. Snyder and E. S. Tobere, Nat. Mater. **7**, 105 (2008).
[2] D. M. Rowe, *CRC Handbook of Thermoelectrics* (CRC Press, New York, 1995).
[3] R. Venkatasubramanian, E. Siivola, T. Colpitts, and B. O'Quinn, Nature **413**, 597 (2001).
[4] T. S. Kim, B. S. Chun, J. K. Lee, and H. G. Jung, *12th International Symposium on Metastable and Nano-Materials (ISMANAM-2005)* (La Maison de la Chimie, Paris, France, 2005), pp. 710.
[5] S. Nakajima, J. Phys. Chem. Solid. **24**, 479 (1963).
[6] T. J. Scheidemantel, J. F. Meng, and J. V. Badding, J. Phys. Chem. Solid. **66**, 1744 (2005).
[7] M. Dresselhaus, G. Dresselhaus, X. Sun, Z. Zhang, S. Cronin, and T. Koga, Phys. Solid State **41**, 679 (1999).
[8] S. S. Hong, W. Kundhikanjana, J. J. Cha, K. Lai, D. S. Kong, S. Meister, M. A. Kelly, Z. X. Shen, and Y. Cui, Nano Lett. **10**, 3118 (2010).
[9] D. Teweldebrhan, V. Goyal, M. Rahman, and A. A. Balandin, Appl. Phys. Lett. **96**, 053107 (2010).
[10] D. Teweldebrhan, V. Goyal, and A. A. Balandin, Nano Lett. **10**, 1209 (2010).
[11] H. Steinberg, D. R. Gardner, Y. S. Lee, and P. Jarillo-Herrero, Nano Lett. **10**, 5032 (2010).
[12] K. M. F. Shahil, M. Z. Hossain, D. Teweldebrhan, and A. A. Balandin, Appl. Phys. Lett. **96**, 153103 (2010).
[13] H. Zhang, C. X. Liu, X. L. Qi, X. Dai, Z. Fang, and S. C. Zhang, Nat. Phys. **5**, 438 (2009).
[14] M. Z. Hassan and C. L. Kane, Rev. Mod. Phys. **82**, 3045 (2010).

[15]J. E. Moore, Nature **464**, 194 (2010).
[16]Y. Xia, D. Qian, D. Hsieh, L. Wray, A. Pal, H. Lin, A. Bansil, D. Grauer, Y. S. Hor, R. J. Cava, and M. Z. Hassan, Nat. Phys. **5**, 398 (2009).
[17]H. Zhang, C. X. Liu, X. L. Qi, X. Dai, Z. Fang, and S. C. Zhang, Nat. Phys. **5**, 438 (2009).
[18]Y. L. Chen, J. G. Analytis, J. H. Chu, Z. K. Liu, S. K. Mo, X. L. Qi, H. J. Zhang, D. H. Lu, X. Dai, Z. Fang, S. C. Zhang, I. R. Fisher, Z. Hussain, and Z. X. Shen, Science **325**, 178 (2009).
[19]H. Steinberg, D. R. Gardner, Y. S. Lee, and P. Jarillo-Herrero, Nano Lett. **10**, 5032 (2010).
[20]J. G. Checkelsky, Y. S. Hor, R. J. Cava, and N. P. Ong, Phys. Rev. Lett. **106**, 196801 (2011).
[21]J. V. Badding, J. F. Meng, and D. A. Polvani, Chem. Mater. **10**, 2889 (1998).
[22]D. A. Polvani, J. F. Meng, N. V. Chandra Shekar, J. Sharp, and J. V. Badding, Chem. Mater. **13**, 2068 (2001).
[23]N. V. Chandra Shekar, D. A. Polvani, J. F. Meng, and J. V. Badding, Phys. B **358**, 14 (2005).
[24]S. V. Ovsyannikov, V. V. Shchennikov, G. V. Vorontsov, A. Y. Manakov, A. Y. Likhacheva, and V. A. Kulbachinskii, J. Appl. Phys. **104**, 053713 (2008).
[25]S. V. Ovsyyannikov and V. V. Shchennikov, Chem. Mater. **22**, 635 (2010).
[26]C.-Y. Li, A. L. Ruoff, and C. W. Spencer, J. Appl. Phys. **32**, 1733 (1961).
[27]L. F. Vereshchagin, E. Y. Atabaeva, and N. A. Bedeliani, Sov. Phys. Solid State **13**, 2051 (1972).
[28]E. Y. Atabaeva, N. A. Bendeliani, and S. V. Popova, Fiz. Tverd. Tela **15**, 3508 (1973) [Sov. Phys. Solid State **15**, 2346 (1974)].
[29]L. G. Khvostantsev, A. I. Orlov, N. K. Abrikosov, and L. D. Ivanova, Phys. Status Solidi A **58**, 37 (1980).
[30]N. Sakai, T. Kajiwara, K. Takemura, S. Minomura, and Y. Fujii, Solid State Comm. **40**, 1045 (1981).
[31]L. G. Khvostantsev, A. I. Orlov, N. K. Abrikosov, and L. D. Ivanova, Phys. Status Solidi A **89**, 301 (1985).
[32]M. Bartkowiak and G. D. Mahan, *18th International Conference on Thermoelectrics* (IEEE, Baltimore, USA, 1999), p. 713.
[33]T. Thonhauser, T. J. Scheidemantel, J. O. Sofo, J. V. Badding, and G. D. Mahan, Phys. Rev. B **68**, 085201 (2003).
[34]T. Thonhauser, Solid State Comm. **129**, 249 (2004).
[35]M. Einaga, Y. Tanabe, A. Nakayama, A. Ohmura, F. Ishikawa, and Y. Yamada, J. Phys. Conf. Ser. **215**, 012036 (2010).
[36]J. L. Zhang, S. J. Zhang, H. M. Weng, W. Zhang, L. X. Yang, Q. Q. Liu, S. M. Feng, X. C. Wang, R. C. Yu, L. Z. Cao, L. Wang, W. G. Yang, H. Z. Liu, W. Y. Zhao, S. C. Zhang, X. Dai, Z. Fang, and C. Q. Jin, Proc. Nat. Acad. Sci. USA **108**, 24 (2011).
[37]C. Zhang, L. Sun, Z. Chen, X. Zhou, Q. Wu, W. Yi, J. Guo, X. Dong, and Z. Zhao, Phys. Rev. B **83**, 140504 (2011).
[38]M. K. Jacobsen, R. S. Kumar, A. L. Cornelius, S. V. Sinogeiken, and M. F. Nicol, *Shock Compression of Condensed Matter Conference Proceedings* (AIP Melville, USA, 2007), Vol. 955, p. 171.
[39]A. Nakayama, M. Einaga, Y. Tanabe, S. Nakano, F. Ishikawa, and Y. Yamada, High Press. Res. **29**, 245 (2009).
[40]M. Einaga, A. Ohmura, A. Nakayama, F. Ishikawa, Y. Yamada, and S. Nakano, Phys. Rev. B **83**, 092102 (2011).
[41]L. Zhu, H. Wang, Y. C. Wang, J. Lv, Y. Ma, Q. L. Cui, Y. Ma, and G. T. Zou, Phys. Rev. Lett. **106**, 145501 (2011).
[42]E. S. Itskevich, L. M. Kashirskaya, and V. F. Kraidenov, Semiconductors **31**, 276 (1997).
[43]A. Polian, M. Gauthier, S. M. Souza, D. M. Trichês, J. Cardoso de Lima, and T. A. Grandi, Phys. Rev. B **83**, 113106 (2011).
[44]I. M. Lifshitz, Sov. Phys. JETP **11**, 1130 (1960).
[45]L. Dagens, J. Phys. F Met. Phys. **8**, 4496 (1978).
[46]L. Dagens and C. Lopez-Rios, J. Phys. F Met. Phys. **9**, 2195 (1979).
[47]A. F. Goncharov and V. V. Struzhkin, Phys. B **385**, 117 (2003).
[48]D. Antonangeli, D. L. Farber, A. H. Said, L. R. Benedetti, C. M. Aracne, A. Landa, P. Söderlind, and J. E. Klepeis, Phys. Rev. B **82**, 132101 (2010).
[49]D. Santamaria-Perez, A. Vegas, C. Muehle, and M. Jansen, J. Chem. Phys. **135**, 054511 (2011).
[50]O. Gomis, R. Vilaplana, F. J. Manjón, P. Rodríguez-Hernández, E. Pérez-González, A. Muñoz, V. Kucek, and C. Drasar, Phys. Rev. B **84**, 174305 (2011).
[51]R. Vilaplana, O. Gomis, F. J. Manjón, A. Segura, E. Pérez-González, P. Rodríguez-Hernández, A. Muñoz, J. González, V. Marín-Borrás, V. Muñoz-Sanjosé, C. Drasar, and V. Kucek, Phys. Rev. B **84**, 104112 (2011).
[52]W. Kullmann, J. Geurts, W. Richter, N. Lehner, H. Rauh, U. Steigenberger, G. Eichhorn, and R. Geick, Phys. Status Solidi B **125**, 131 (1984).
[53]H. Köhler and C. R. Becker, Phys. Status Solidi B **61**, 533 (1974).
[54]W. Richter, H. Köhler, and C. R. Becker, Phys. Status Solidi B **84**, 619 (1977).
[55]H. Rauh, R. Geick, H. Köhler, N. Nücker, and N. Lehner, J. Phys. C Solid State Phys. **14**, 2705 (1981).
[56]J. Zhang, Z. Peng, A. Soni, Y. Zhao, Y. Xiong, B. Peng, J. Wnag, M. S. Dresselhaus, and Q. Xiong, Nano Lett. **11**, 2407 (2011).
[57]G. Zhang, H. Qin, J. Teng, J. Guo, Q. Guo, X. Dai, Z. Fang, and K. Wu, Appl. Phys. Lett. **95**, 053114 (2009).
[58]S. Y. F. Zhao, C. Beekman, L. J. Sandilands, J. E. J. Bashucky, D. Kwok, N. Lee, A. D. LaForge, S. W. Cheong, and K. S. Burch, Appl. Phys. Lett. **98**, 141911 (2011).
[59]W. Cheng and S. F. Ren, Phys. Rev. B **83**, 094301 (2011).
[60]W. Kraus and G. Nolze, J. Appl. Crystallogr. **29**, 301 (1996).
[61]J. Rodriguez-Carvajal, Phys. B **192**, 55 (1993).
[62]G. J. Piermarini, S. Block, and J. D. Barnett, J. Appl. Phys. **44**, 5377 (1973).
[63]D. Errandonea, Y. Meng, M. Somayazulu, and D. Hausermann, Phys. B **355**, 116 (2005).
[64]K. Syassen, High Press. Res. **28**, 75 (2008).
[65]P. Hohenberg and W. Kohn, Phys. Rev. **136**, B864 (1964).
[66]G. Kresse and J. Hafner, Phys. Rev. B **47**, 558 (1993); **49**, 14251 (1994); G. Kresse and J. Furthmüller, Comput. Mater. Sci. **6**, 15 (1996); Phys. Rev. B **54**, 11169 (1996).
[67]P. E. Blöchl, Phys. Rev. B **50**, 17953 (1994); G. Kresse and D. Joubert, *ibid.* **59**, 1758 (1999).
[68]J. P. Perdew, A. Ruzsinszky, G. I. Csonka, O. A. Vydrow, G. E. Suseria, L. A. Constantin, X. Zhou, and K. Burke, Phys. Rev. Lett. **100**, 136406 (2008).
[69]A. Mujica, A. Rubio, A. Muñoz, and R. J. Needs, Rev. Mod. Phys. **79**, 863 (2003).
[70]M. A. Blanco, E. Francisco, and V. Luaña, Comput. Phys. Comm. **158**, 57 (2004).
[71]K. Parlinski, computer code PHONON. See [http://wolf.ifj.edu.pl/phonon].

[72]See Supplemental Material at http://link.aps.org/supplemental/10.1103/PhysRevB.84.184110 for calculation details regarding IR-active modes.
[73]R. J. Angel, Rev. Mineral Geochem. **41**, 35 (2000).
[74]M. Cardona, High Press. Res. **24**, 17 (2004); Phys. Status Solidi B **241**, 3128 (2004).
[75]C. Ulrich, M. A. Mroginski, A. R. Goñi, A. Cantarero, U. Schwarz, V. Muñoz, and K. Syassen, Phys. Status Solidi B **198**, 121 (1996).
[76]A. M. Kubelikov, H. P. Olijnyk, A. P. Jephcoat, Z. Y. Salaeva, S. Onari, and K. R. Allakverdiev, Phys. Status Solidi B **235**, 517 (2003).